Applied Catalysis B: Environmental 210 (2017) 1–13

Contents lists available at ScienceDirect

Applied Catalysis B: Environmental

journal homepage: www.elsevier.com/locate/apcatb

Exploring pretreatment effects in Co/SiO_2 Fischer-Tropsch catalysts: Different oxidizing gases applied to oxidation-reduction process

Jian Cai, Feng Jiang, Xiaohao Liu *

Department of Chemical Engineering, School of Chemical and Material Engineering, Jiangnan University, 214122 Wuxi, China

ARTICLE INFO

Article history:
Received 3 January 2017
Received in revised form 9 March 2017
Accepted 12 March 2017
Available online 16 March 2017

Keywords:
Cobalt nanoparticles
Silica
Reduction-oxidation-reduction treatment
Water vapor
Oxygen

ABSTRACT

The influence of reduction-oxidation-reduction (ROR) pretreatment on 20% Co/SiO_2 has been investigated using different oxidizing gases including water vapor and oxygen in the oxidation step. In this study, the evolution concerning the SiO_2 structure and the cobalt phase and morphology is clearly elucidated at each step of reduction, oxidation and subsequent re-reduction. It is demonstrated that ROR treatment using both oxygen and water vapor decreases the average cobalt particle size. However, the catalytic performance affected in FTS is considerably different. ROR treatment in oxygen results in an increase in catalytic activity. In contrast, the water vapor applied in oxidation step obviously deactivates cobalt catalyst and enhances selectivity of methane. The resulting deactivation is ascribed to the promoted formation of irreducible cobalt silicate through the reaction between water vapor caused surface Si—OH groups and oxidized cobalt (CoO) in spite of unchanged surface area and pore structure on SiO_2. The characterization data reveals that the re-dispersion of cobalt particles occurs at oxidation step rather than the re-reduction step. In addition, the results indicate that the ROR treatment reducing the cobalt particle size depends on its initial size as no re-dispersion can be observed in the case of particles smaller than about 11 nm. Furthermore, the water vapor shows more effective re-dispersion in cobalt particles compared with the use of oxygen. This study provides fundamental insights into the control of catalytic activity, product selectivity, and catalyst stability over supported cobalt catalysts by understanding the evolution of catalyst structure through ROR treatment in different chemical environment.

1. Introduction

The production of fuels and chemicals from any combustible carbon-containing source, including coal, natural gas, biomass, or garbage, would be an attractive alternative to unstable petroleum supplies [1–5]. The Fischer-Tropsch synthesis (FTS) has the advantages for producing such desired super-clean motor fuels and chemicals without the production of the environmentally harmful compounds encountered in direct hydrogenation. In contrast to the FTS of iron-based catalysts, the cobalt catalysts can convert CO and H_2 into higher-molecular-weight hydrocarbons with the merits of a milder operating temperature, a longer lifetime, and a negligible water-gas-shift (WGS) activity, which is now utilized on a large scale in several commercial plants [6–10].

Although the FTS has been studied over 90 years, there still exists room for improving the efficiency of this process by understanding of working mechanism on the cobalt catalysts. The process could be improved in several areas. Among them, the most important aspect is to develop a highly stable catalyst and search for an efficient approach to regenerate the catalyst for the use of a prolonged time. In the case of cobalt catalysts, the deactivation mechanisms reported in literature includes sintering of cobalt nanoparticles, oxidation of active cobalt metal into inactive cobalt oxide at high water partial pressure, formation of irreducible cobalt-support compounds, carbon effects (e.g., heavy hydrocarbons accumulation on active sites, and carbidization to inactive cobalt carbide), and poisoning [11–17]. Sintering leading to the cobalt particle growth is still a topic that has received much attention from both industrial and academic sides, which has been identified to be a key factor in catalyst deactivation.

Since the catalytic activity is proportional to the particle size of the supported cobalt nanoparticles, the strategy of re-activating catalysts is to re-disperse the large cobalt nanoparticles resulting from sintering/agglomeration. The re-dispersion can lead to smaller particles typically resulting in higher activities for recycling of supported cobalt catalysts, which can be realized through the conventional reduction-oxidation-reduction (ROR) process [18]. The ROR treatment reported in literatures does often utilize the oxygen as oxidant, which can reactivate the catalysts and enhance the activity from not only the re-dispersion of large cobalt

* Corresponding author.
E-mail address: liuxh@jiangnan.edu.cn (X. Liu).

http://dx.doi.org/10.1016/j.apcatb.2017.03.036
0926-3373/

nanoparticles but also the removal of accumulated heavy hydrocarbons and deposited carbon, and the reduction of surface oxidized cobalt and inactive cobalt carbide. Thereby, the ROR process is an attractive method for the regeneration to attain the recycling use of cobalt catalysts. The metal re-dispersion strategy for recycling of various supported metal catalysts has been reviewed extensively [19–24]. It can be summarized that the studies are mostly focusing on the oxygen as oxidant which is used to oxidize the reduced metallic Co to investigate its effects on the structural and morphological changes and the reducibility during the ROR treatment. For the cobalt-based FTS, a large amount of water is produced leading to a high partial pressure of water in the reactor under the industrial operating conditions due to the absence of WGS reaction to consume the formed water unlike the case of iron-based FTS [6,7,25–27]. Despite tremendous efforts devoted to water effects in the cobalt-based FTS, the water is always introduced as a co-fed gas during the FTS reaction. Since the added water can affect not only the catalyst structure, but also the adsorption and dissociation of CO and H_2, and the secondary reactions of olefins [28], it's hard to clarify the resulting catalytic performances comes from which pathway. Therefore, it impels us to be aware of the use of water oxidant as an oxygen substitute for the ROR treatment to uncover the deactivation behavior due to the presence of water prior to the FTS reaction, which is of great importance to make it clear for providing the efficient manner of minimizing water effects during the FT reaction.

In order to introduce different water content for testing its effects, we apply the nitrogen gas to carry water steam into the reactor by changing the temperature of evaporator after the first reduction step. A more detailed investigation of the process is taken to understand the exact reason for the resulting catalytic performance, which includes the measurements of the changes in the support/catalyst textural and surface properties, average cobalt particle size, and reduction behavior of each treatment step in the ROR process. These changes can be used to draw conclusions on the main reasons for catalyst deactivation from the water effects. In this study, for the purpose of comparison, the corresponding oxidation step by using oxygen as an oxidant is also investigated in details to elucidate the changes mentioned above, where the monometallic 20 wt% Co/SiO_2, as a model catalyst to exclude the effects of promoter, are used with the different initial sizes obtained by preparing the catalysts from regulating cobalt precursors, calcination gases, and the space velocity of calcination.

2. Experimental

2.1. Catalyst preparation

The supported cobalt catalysts were prepared by an incipient wetness impregnation method following our previous work [29]. Briefly, to obtain 20 wt% Co in the final Co/SiO_2 catalyst, required amount of $Co(NO_3)_2{\cdot}6H_2O$ aqueous solution was impregnated to SiO_2 (Fujisilicia Q-15) support. After impregnation, the sample was dried slowly in a rotary evaporator to remove the excess water and then in an oven at 120 °C for 12 h followed by calcined in air with a heating rate of 2 °C min^{-1} at 400 °C for 4 h. To obtain different initial sizes of Co particles, the other two cobalt precursors including $CoCl_2{\cdot}6H_2O$ and $Co(OAc)_2{\cdot}4H_2O$ were also used to prepare the Co/SiO_2 catalysts, and labeled as $Co\text{-}Cl/SiO_2$ and $Co\text{-}Ac/SiO_2$, respectively. It is should be noted that, in the case of $Co\text{-}Cl/SiO_2$, the calcination step was operated at 500 °C for 4 h in order to decompose the cobalt precursor completely. Furthermore, the initial sizes of Co particles were regulated by calcination in different gases (air or nitrogen) and by using different space velocity of nitrogen, and the catalysts were labeled as $Co/SiO_2\text{-}N_2\text{-}X$ where X is the space velocity of N_2. The calcined samples were crushed and sieved to 40–60 mesh for the FTS reaction.

2.2. Catalyst characterization

In general, the catalysts were characterized by physical adsorption of nitrogen, XRD, TEM, H_2-TPR, FTIR, and Raman. Prior to the characterization of reduced, R-N_2 and R-H_2O treated samples, the samples were passivated in the flowing gas of 1% O_2/N_2 at RT for 1 h.

The specific surface areas and total pore volume were determined from N_2 adsorption/desorption isotherms at −196 °C using an automated surface area and pore size analyzer (Micromeritics ASAP 2020). Prior to the measurement, the sample was degassed at 150 °C for 4 h under vacuum. The specific surface area was determined according to the BET method in the relative pressure range of 0.01-0.3. The pore size and pore volume were calculated based on the Barrett-Joyner-Halenda (BJH) method using the desorption branches of the N_2 isotherms.

The powder X-ray diffraction (XRD) patterns were recorded by a Bruker AXS D8 Advance diffractometer using Cu(Kα) radiation (λ = 1.5406 Å) at 40 kV and 40 mA at room temperature (RT) with 0.02° step size and 0.4 s step time from 5 to 90°. The average Co_3O_4 crystallite size was calculated from the Scherrer equation using a Co_3O_4 XRD peak at 2θ = 37.0°. Metallic Co crystallite size was calculated by the Scherrer equation using a Co XRD peak at 2θ = 44.4° or by the formula $d(Co^0) = 0.75 \times d(Co_3O_4)$ if the crystallite was Co_3O_4.

Transmission electron microscopic (TEM) images of the samples were obtained by using a JEOL JEM-2100 microscope operating at 200 kV. The samples were prepared by dropwise addition of the dilute catalyst suspension on a carbon-coated copper TEM grid followed by the evaporation of the solvent ethanol. The cobalt particle histograms were obtained via evaluating several hundred detected cobalt particles from the TEM images.

H_2 temperature-programmed reduction (H_2-TPR) was recorded by an automated chemisorption analyzer (TP5076 TPD/TPR) using a gas chromatograph equipped with a thermal conductivity detector. Typically, prior to the TPR measurements, 50 mg samples were treated at 200 °C in a N_2 flow for 1 h to remove traces of water and impurities and then cooled to RT. The gas mixture 5% H_2/N_2 was introduced to the sample bed until a stable baseline was reached with a flow rate of 30 mL/min. The H_2 TPR curve was recorded from 30 to 800 °C at a heating rate of 10 °C min^{-1}. The consumption of H_2 was calculated from the TPR peak area calibrated by injecting H_2 of precise 100 μL into the TPR analyzer and repeating twice. The reducibility of cobalt catalysts was calculated from the H_2 consumption before 400 °C.

The Fourier transform infrared spectroscopy (FTIR) spectra were recorded with a Nicolet 6700 FTIR spectrophotometer in the range of approximately 4000–500 cm^{-1} with a resolution of 2 cm^{-1}. The specimens for FTIR measurements were prepared by grinding the samples with KBr together, and then compressed into thin pellets under 10 MPa.

Raman spectra were acquired using a Renishaw Micro Raman spectrometer equipped with a confocal microscope and a laser wavelength of 785 nm. The laser line at 785 nm was removed from the backscattered light using an edge filter, and the filtered radiation was detected by a CCD detector after passage dispersion by a grating. Samples were placed on the glass slide and the spectra were obtained at room temperature.

2.3. Catalyst tests

FTS reaction was carried out in a tubular flow fixed-bed reactor operating at a total pressure of 1 MPa, 230 °C, GHSV = 4.5 L g_{cat}^{-1} h^{-1}, and $H_2/CO = 2$ molar ratio. In general, 1 g

catalyst diluted with 3.1 g quartz sand was packed into a stainless steel reactor (i.d. of 8.0 mm). For the R-treated catalyst, the catalyst was pre-reduced in situ at a relatively high temperature of 500 °C in H_2 for 4 h under atmospheric pressure in order to make sufficient reduction of cobalt phase. The space velocities of flowing gases in the present study are all designed as 4.5 L g_{cat}^{-1} h^{-1}. Then the catalyst was cooled to 200 °C and a flow of premixed syngas was gradually fed into the reactor at a certain flow rate. When the pressure reached 1 MPa, the temperature was slowly increased to the designed reaction temperature of 230 °C to start the FTS reaction.

For the ROR treated catalyst, the pre-reduced catalyst was further oxidized and subsequently re-reduced before the FTS test. In a typical ROR process, after the catalyst was reduced firstly at 500 °C for 4 h, the temperature was decreased to room temperature and the reduced sample was then passivated in 1% O_2/N_2 for 2 h followed by oxidation in an oven at 300 °C (2 °C min^{-1}) in static air for 4 h. Finally, the oxidized sample was re-reduced in situ at 300 °C in H_2 for 4 h under atmospheric pressure before starting the FTS reaction. It should be noted that the re-reduction temperature is designed at an obviously lower value compared to that of the first reduction at 500 °C, which is considered as the sintering of Co nanoparticles at the re-reduction stage possibly occurred at a high temperature and thus led to incorrect evaluation of the re-dispersion of Co nanoparticles resulting from the OR treatment. In the oxidation step, other gases including N_2 and water vapor were also used in this study, which were labeled as R-N_2-R and R-H_2O(Y)-R where the Y was the temperature of vaporizer chamber. In the case of N_2, the pre-reduced sample was treated in situ in flowing N_2 without the passivation step. In the case of water vapor, it was introduced into the reactor by a carrier of N_2 bubbling into a sealed triangular flask containing water that was set in the oil bath of constant temperature at 60 °C, 80 °C and 100 °C, respectively.

Gaseous products were analyzed online by a gas chromatography (Agilent GC 7820A). CO_2, H_2, CO, N_2, CH_4 were measured using a TCD detector with a Porapak Q column and a 5A molecular sieve column. C_1-C_6 hydrocarbons were analyzed with a Rt-Q-BOND column using an FID detector. 3% of N_2 was used as an internal standard to calculate the CO conversion and product selectivity. The liquid products collected together from hot and ice-cooled traps were analyzed offline by a gas chromatography GC-2014 AFSC (Shimadzu) equipped with an HP-1 capillary column. The CO conversion and product selectivity were obtained as the FTS reaction was stable.

3. Results and discussion

3.1. Effects of oxidizing gas in ROR process

The BET surface area, average pore size and total pore volume of silica support and supported cobalt catalysts are given in Table 1. The S_{BET}, D_{pore} and V_{pore} for the silica support are 187.4 m^2 g^{-1}, 25.2 nm and 1.18 cm^3 g^{-1}, respectively. With the loading of cobalt, the S_{BET}, D_{pore} and V_{pore} significantly decreases to 137.1 m^2 g^{-1}, 20.5 nm and 0.72 cm^3 g^{-1}, respectively. The further reduction-oxidation (RO) treatment results in slight changes in surface area and pore properties over different oxidizing gases and conditions. At the same time, the N_2 adsorption-desorption isotherms of parent silica demonstrate mainly adsorption at high pressures (p/p_0 = 0.9–0.95) before and after Co loading due to the filling of silica inter-globular spaces as shown Fig. S1. However, the particle size of metallic cobalt is remarkably changed after the reduction of cobalt oxide (R) followed by subsequent oxidation step using N_2, air, and water. One can see that the followed treatment of nitrogen does not change the cobalt particle size obviously from 18.5 to 16.8 nm. In contrast, the air treatment shows a marked decrease in the particle size from 18.5 to 11.4 nm. Interestingly, the treatment with water vapor carried by nitrogen displays the significantly smaller particle size from 16.8, 9.6 to 8.1 nm with a correspondingly higher temperature of the evaporator from 60, 80 to 100 °C despite that the relatively low temperature at 60 °C does not bring about the change of cobalt particle size. It is concluded that the reduction-oxidation treatment could reduce the particle size of Co_3O_4/Co with the oxidation process as the crucial step regardless of the air or water vapor as oxidizing gas. Compared with air, the water vapor is more efficient to re-disperse cobalt species and reduce the crystallite size over Co/SiO_2 catalysts.

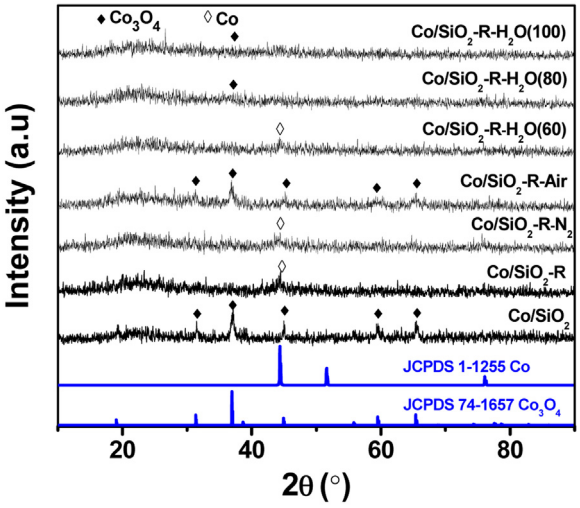

Fig. 1. XRD patterns of the catalysts with different oxidizing gases in the ROR treatment.

The XRD patterns of catalysts with different oxidizing atmosphere in the ROR-treatment are presented in Fig. 1 and the average particle size of Co_3O_4/Co calculated from XRD patterns are listed in Table 1 as well. The broad peak at around 2θ = 22° is attributed

Table 1
Textural properties, Co and Co_3O_4 size calculated by XRD and TEM methods of the catalysts.

Catalyst	S_{BET}(m^2/g)	D_{pore}(nm)	V_{pore}(cm^3/g)	Co particle size, nm		Co_3O_4 particle size, nm		Percentage of reduction (%)
				by XRD[a]	by TEM	by XRD[b]	by TEM	
SiO_2	187.4	25.2	1.18	–	–	–	–	–
Co/SiO_2-calcined	137.1	20.5	0.72	18.5[c]	16.7[c]	24.7	22.3 ± 4.1	60.8
Co/SiO_2-R-N_2	148.4	19.2	0.71	16.8	18.4 ± 4.0	–	–	–
Co/SiO_2-R-Air	145.1	19.0	0.69	11.4[c]	12.5[c]	15.2	16.7 ± 4.3	47.6
Co/SiO_2-R-H_2O(60)	143.2	19.3	0.69	17.2	16.8 ± 4.3	–	–	–
Co/SiO_2-R-H_2O(80)	174.9	13.7	0.61	–	9.6[c]	–	12.8 ± 2.8	24.3
Co/SiO_2-R-H_2O(100)	150.7	17.6	0.66	–	8.1[c]	–	10.8 ± 3.3	22.7

[a] Calculated from the Scherrer equation from the Co reflection at $2\theta = 44.4°$.
[b] Calculated from the Scherrer equation from the Co_3O_4 reflection at $2\theta = 37.0°$.
[c] Calculated from Co_3O_4 particle, $d(Co) = 0.75 \times d(Co_3O_4)$.

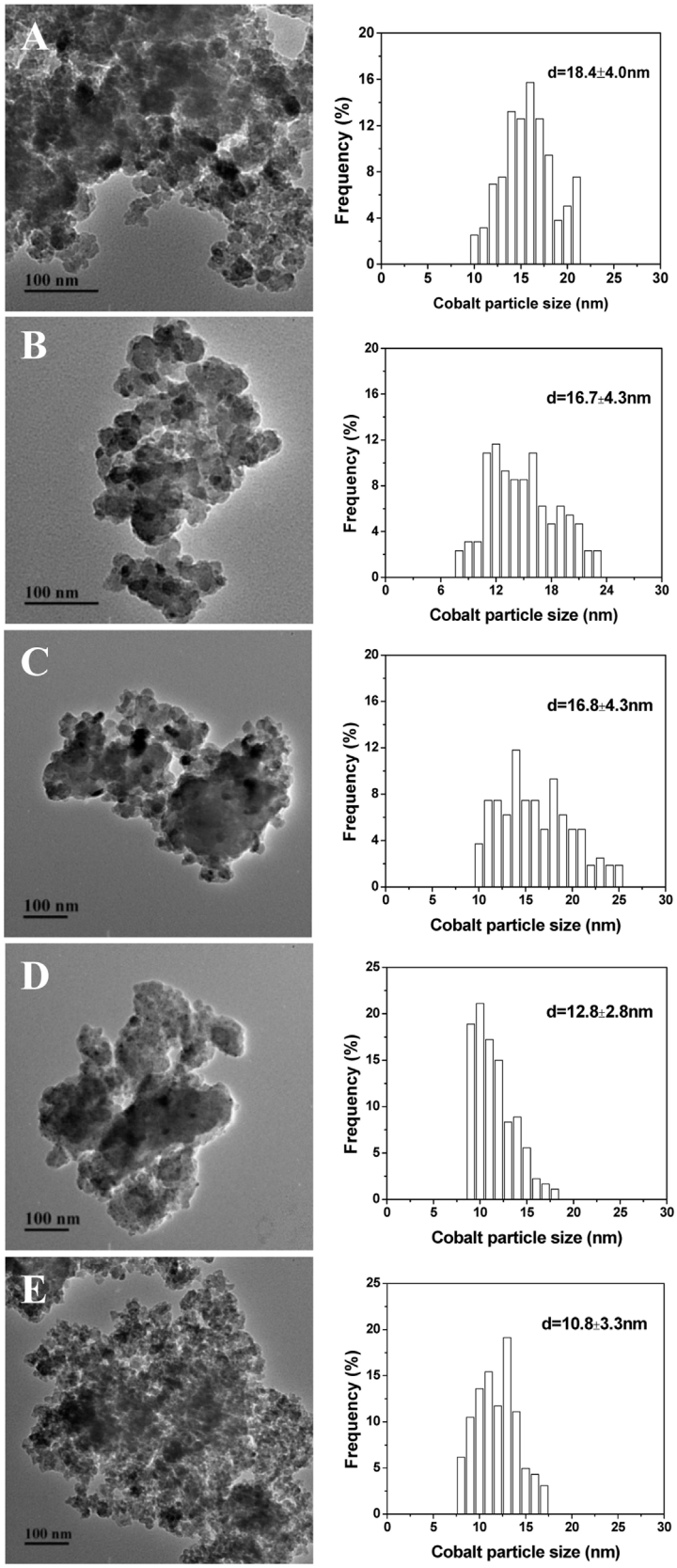

Fig. 2. TEM images and corresponding PSD of the catalysts of A) Co/SiO_2-R-N_2, B) Co/SiO_2-R-Air, C) Co/SiO_2-R-H_2O(60), D) Co/SiO_2-R-H_2O(80) and E) Co/SiO_2-R-H_2O(100).

to the amorphous silica support. For the calcined Co/SiO_2, the XRD patterns located at 31.4°, 37.0°, 45.0°, 59.5°, and 65.4° are observed, which are assigned to Co_3O_4 (JCPDS 74-1657). After pre-reduction, the XRD patterns appear at 44.4° and 51.7° indicating the presence of metallic cobalt (JCPDS 1-1255), which are typically obtained through the reduction of Co_3O_4. If the oxidation step in

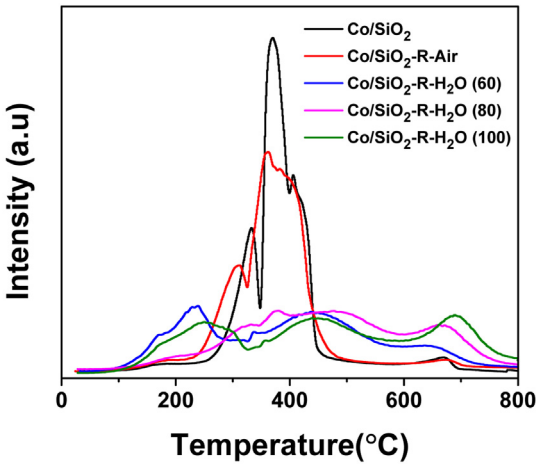

Fig. 3. H_2-TPR profiles of the pre-reduced cobalt catalysts treated with different oxidizing gases.

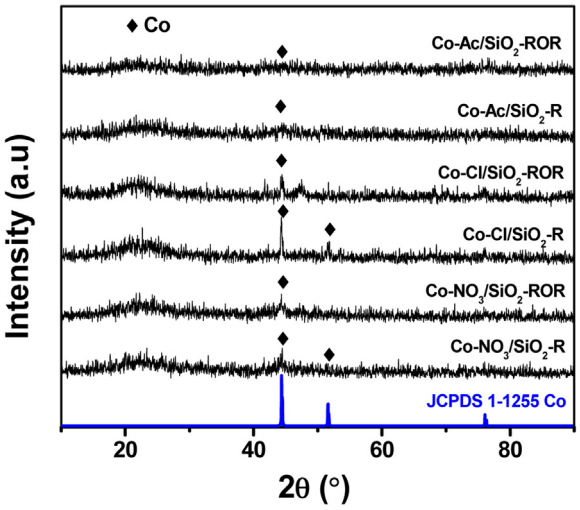

Fig. 4. XRD patterns of the R and ROR treated catalysts prepared with different precursors.

ROR treatment makes use of the N_2 gas (i.e. Co/SiO_2-R-N_2 sample), the metallic cobalt could not be oxidized exhibiting a particle size of 16.8 nm. When the pre-reduced cobalt catalyst is treated in static air, the metallic Co has been oxidized whereas the intensity of Co_3O_4 patterns is weakened compared to Co/SiO_2 suggesting that the particle size of Co_3O_4 decreases after the R-air treatment. In the case of water vapor treated samples, the amount of water vapor at 60 °C is insufficient to oxidize all the metallic cobalt resulting in a weak XRD peak of Co with an average size of 17.2 nm, approximate to Co/SiO_2-R-N_2 sample. As the temperature of water vapor is increased to 80 °C, the cobalt has been oxidized and re-dispersed with only weak XRD pattern at 37.0° assigned to Co_3O_4. There is even no discernible pattern in the sample treated by water vapor of 100 °C. The XRD patterns of those two samples are too weak to calculate the particle size.

Fig. 2 exhibits the TEM images and corresponding particle size distribution (PSD) of the RO treated Co/SiO_2 catalysts with different oxidizing gases. When the pre-reduced catalysts are treated with N_2 and N_2-carried water vapor at 60 °C, the average particle sizes of Co/SiO_2-R-N_2 and Co/SiO_2-R-H_2O (60) show the similar values at 18.4 and 16.8 nm as the metallic Co state. When air or abundant water vapor with a higher vaporizing temperature is introduced into the RO process, the dispersion of cobalt oxide is obviously improved and the particle size is smaller especially for the sample treated in 100 °C water vapor. The average particle size obtained via evaluating several hundred detected cobalt particles from the TEM images is provided in Table 1 as well, which is in accordance with that calculated by the XRD patterns. Specially, the average particle sizes of Co/SiO_2-R-H_2O(80) and Co/SiO_2-R-H_2O(100) samples which could not be calculated from the corresponding XRD patterns can be measured by TEM, which are 12.8 ± 2.8 and 10.8 ± 3.3 nm, respectively. The smaller particle size and more dispersed crystallites in R-Air, R-H_2O treated samples are well in agreement with the XRD results.

Fig. 3 shows the H_2-TPR profiles for the calcined, R-Air, and R-H_2O(60, 80, 100) treated samples. The reduction profile of the calcined sample is characterized by a broad reduction peak from 340 to 450 °C coupled with a narrow, lower temperature shoulder from 280 to 340 °C and a tiny peak above 650 °C. The first peak with the maximum temperature of 330 °C indicates the reduction of Co_3O_4 to CoO [30]. The second broader peak between 340 and 450 °C is ascribed to two different species with maxima at ca. 370 °C and at ca. 410 °C. The maximum at 370 °C is attributed to the reduction of CoO with weak interaction with the support to metallic Co, while the species reducing at slightly higher temperature might have a stronger interaction with the silica surface [31]. The last small peak at ca. 670 °C might be due to the reduction of cobalt silicate [32]. This cobalt silicate is hardly reduced under normal reduction condition prior to FTS reaction. When the Co/SiO_2 is subjected to reduction-oxidation (Air) treatment, the reduction peaks shifting to lower temperatures indicate the easier reduction. In contrast to the above samples, the water vapor treated samples show a marked increase in peak intensity above 650 °C assigned to the reduction of cobalt silicate and the peak intensity becomes stronger as the increase of evaporator temperature.

3.2. *Effects of initial size in ROR process*

To further study the effect of initial size of supported cobalt oxide on their ROR behavior, three different precursors including $Co(NO_3)_2{\cdot}6H_2O$, $CoCl_2{\cdot}6H_2O$, $Co(OAc)_2{\cdot}4H_2O$ were used to alter the cobalt oxide particle size over Co/SiO_2 catalyst. As indicated by the XRD patterns of the three calcined samples in Fig. S2, large crystallites of Co_3O_4 of 38.3, 24.7 and 19.5 nm are obtained over Co-Cl/SiO_2, Co-NO_3/SiO_2, and Co-Ac/SiO_2 catalyst, respectively. The change of cobalt particle size during the R and ROR treatment over catalysts with different initial Co_3O_4 size is summarized in Table 2. The precursor containing chlorine yields much bigger particle size than other precursors, while the acetate precursor usually results in smaller particle sizes. Fig. 4 exhibits the XRD patterns of the pre-reduced (R) and reduction-oxidation(Air)-reduction (ROR) treated samples with different precursors. The peaks at 2θ values of 44.4° and 51.7° indicate the presence of metallic cobalt, and the crystal sizes calculated from the XRD peak at 44.4° are listed in Table 2. For the Co-Cl/SiO_2 sample with a larger initial Co_3O_4 size of 38.3 nm, the peaks of Co are obviously visible after R treatment. After the ROR cycle, the peaks are apparently weak, which indicates a sharply reduced Co particle size from 35.2 to 24.7 nm. For the Co-NO_3/SiO_2 sample with a medium Co_3O_4 size of 24.7 nm, the crystal size of Co decreases to a smaller extent from 20.6 to 15.2 nm. As expected, the Co-Ac/SiO_2 sample with a smaller initial Co_3O_4 size of 19.5 nm exhibits the slight change in Co crystal size from 14.7 to 13.1 nm due to the ROR treatment. Therefore, the cobalt particle size reducing effect of ROR treatment is strongly dependent on the initial particle size, and the catalyst with larger original cobalt oxide size has a larger decrease extent. Besides, the theoretical sizes of Co NPs which are calculated from the Co_3O_4 NPs size are 28.7, 18.5, and 14.6 nm for Co-Cl/SiO_2, Co-NO_3/SiO_2, and Co-Ac/SiO_2 catalyst in Table 2, respectively. The higher values of real size of Co NPs (35.2,

Table 2
Change of cobalt particle size during the R and ROR treatment.

Sample	d(Co_3O_4)[a],nm	d(Co)[b],nm	d(Co)-R, nm		d(Co)-ROR, nm		Percentage of reduction (%)[d]
			by XRD[c]	by TEM	by XRD[c]	by TEM	
Co-Cl/SiO_2	38.3	28.7	35.2	32.8 ± 4.7	24.7	24.2 ± 5.8	2.0 (24.8)[e]
Co-NO_3/SiO_2	24.7	18.5	20.6	20.2 ± 4.5	15.2	15.7 ± 4.3	60.8 (47.6)[e]
Co-Ac/SiO_2	19.5	14.6	14.7	16.0 ± 3.9	13.1	15.5 ± 4.1	31.3 (27.7)[e]

[a] Calculated from the Scherrer equation from the Co_3O_4 reflection at $2\theta = 37.0^\circ$.
[b] $d(Co) = 0.75 \times d(Co_3O_4)$.
[c] Calculated from the Scherrer equation from the Co reflection at $2\theta = 44.4^\circ$.
[d] Values for the fresh calcined catalysts.
[e] Values for the RO-treated catalysts.

20.6, and 14.7 nm, respectively) in the R-treated samples imply an aggregation of Co NPs during the catalyst reduction, especially for the two Co-Cl/SiO_2 and Co-NO_3/SiO_2 samples.

The TEM images and corresponding PSD histograms of the R- and ROR-treated catalysts are presented in Fig. 5 and the average sizes of Co NPs measured from TEM images are summarized in Table 2 as well. Clearly, the Co NPs are dispersed randomly on the amorphous silica. After the R-treatment, however, the agglomeration of Co NPs is observed during the reduction process, especially for the Co-Cl/SiO_2 and Co-NO_3/SiO_2 samples, which is in accordance with the XRD results. After the ROR-treatment, the agglomeration of Co NPs is effectively reduced and the particle size of Co shifts toward a smaller value with the decreasing order of Co-Cl/SiO_2 > Co-NO_3/SiO_2 > Co-Ac/SiO_2. Moreover, the average particle size calculated from TEM images is also in accordance with that estimated by XRD. All the samples have a broad size distribution of ±4–5 nm matched with the broad XRD patterns of cobalt metal in Fig. 4.

Even smaller initial Co_3O_4 particles are further obtained by tuning the calcination environment, and the change of particle size during the ROR process are listed in Table S1. In contrast to the large average particle size of Co_3O_4 at 24.7 nm obtained at calcination in static air, the cobalt nitrate precursor calcined in flowing N_2 produces much smaller particles of Co_3O_4 as indicated by the XRD patterns in Fig. S3. And the Co_3O_4 particle size decreases from 15.1, 14.4 to 13.4 nm with an increase in the space velocity of N_2 from 2500, 5000 to 10,000 h^{-1}. In the R and ROR treated catalysts, only weak metallic cobalt diffraction peak at 2θ value of 44.4° can be observed in Fig. S4. Different from the cobalt catalysts prepared with three different precursors, the cobalt catalysts calcined in flowing N_2 do not display the obvious change in cobalt particle size distribution between the R and ROR treatment as confirmed by the TEM images in Fig. 6. Moreover, the ROR treatment resulted decrease in cobalt particle size becomes more and more negligible on smaller initial cobalt particle size. As observed in Table S1, the values for cobalt particle sizes calculated from the XRD data are well in accordance with those from TEM images. It should be noted from Fig. 6 that the higher space velocity of N_2 results in better dispersion of cobalt on the SiO_2 support, which does not exhibit the agglomeration of Co NPs compared to the case of calcination in static air.

3.3. Comparison of catalytic results over R and ROR treated catalysts

The catalytic results studying the impact of oxidation gas in the ROR treatment are provided in Table 3. As expected, the R-N_2-R and RR treatment could not alter the catalytic activity for both of the treatments are unable to alter cobalt particle size. The R-Air-R treatment could enhance the catalytic activity from 49.9% to 59.3% due to the smaller cobalt particle size and the easier reduction of cobalt oxides. If water vapor is introduced in the treatment, the catalytic activity is slightly improved to 53.4% and then decreases linearly to 28.4% as the increase of the space velocity of water vapor to result in the promoting formation of hardly reducible cobalt silicate. Different from the R-Air-R treated catalysts, the selectivity of CH_4 gradually increases from 8.5% to 14.4% in parallel with a decrease of C_{5+} hydrocarbons from 84.5% to 69.9% over the R-H_2O(100)-R treated sample. However, the selectivity to lower olefins ($C_2^=$–$C_4^=$) obviously increases from 3.3% to 9.0%.

The catalytic results of the R and ROR treated supported cobalt catalysts with different precursors are listed in Table 4. Despite of the varied precursors, the catalytic activity is highly enhanced from 6.5% to 59.3% as the size of Co NPs reduces from 35.2 to 15.2 nm indicating a strong dependence of catalytic activity on Co NPs size. The CO conversion is doubled from 6.5% to 13.4% with the Co NPs size decreasing from 35.2 to 24.7 nm over Co-Cl/SiO_2 catalyst. The Co-NO_3/SiO_2 catalyst with a medium decrease in Co NPs size results in a medium increase in CO conversion from 49.9% to 59.3%. As expected, the Co-Ac/SiO_2 sample possessing similar size of Co NPs after the R and ROR treatment yields similar CO conversions of 54.6% and 56.3%, respectively. When the catalyst experiences a second ROR treatment, the catalytic activity could not be further elevated indicating a negligible change of Co NPs size during the second ROR treatment. Therefore, the increase or decrease of catalytic activity is directly related to the reduced or enlarged Co NPs size over the catalyst prepared by the same precursor.

Table S2 shows the effects of calcination environment on the improvement of catalytic performance by ROR treatment. The Co/SiO_2 catalyst calcined in pure N_2 at a space velocity of 2500 h^{-1} gives a much higher CO conversion of 72.3% than that in static air (49.9%, Table 3). Although the CO conversion is further increased to 79.6% with an increase in the calcination space velocity of N_2 from 2500 to 10,000 h^{-1}, the catalytic activity could not be further improved by ROR treatment due to the smaller initial Co NPs size. In addition, the ROR treatment even decreases the CO conversion compared with R treated Co/SiO_2 catalyst. Different from the case of 2500 or 5000 h^{-1} calcined samples, the one calcined at 10,000 h^{-1} exhibits slightly higher C_{5+} selectivity after OR treatment. The decreased selectivity to C_{5+} is due to the observable reduction of cobalt particle size that is unfavorable for chain growth. However, the Co/SiO_2-10,000 h^{-1} has a lower initial Co particle size, which results in a negligible change of particle size after OR treatment thereby the selectivity to methane and C_{5+} varies in a small range.

3.4. Discussion

The carbene mechanism has been proposed and generally accepted in the FTS over cobalt-based catalysts where the metallic cobalt is regarded as the active sites [6,28,33]. Over the past long history of FTS, the relationship between the catalyst structures and catalytic performances has been intensively investigated to elucidate the effects of various parameters in FTS [34–36]. The

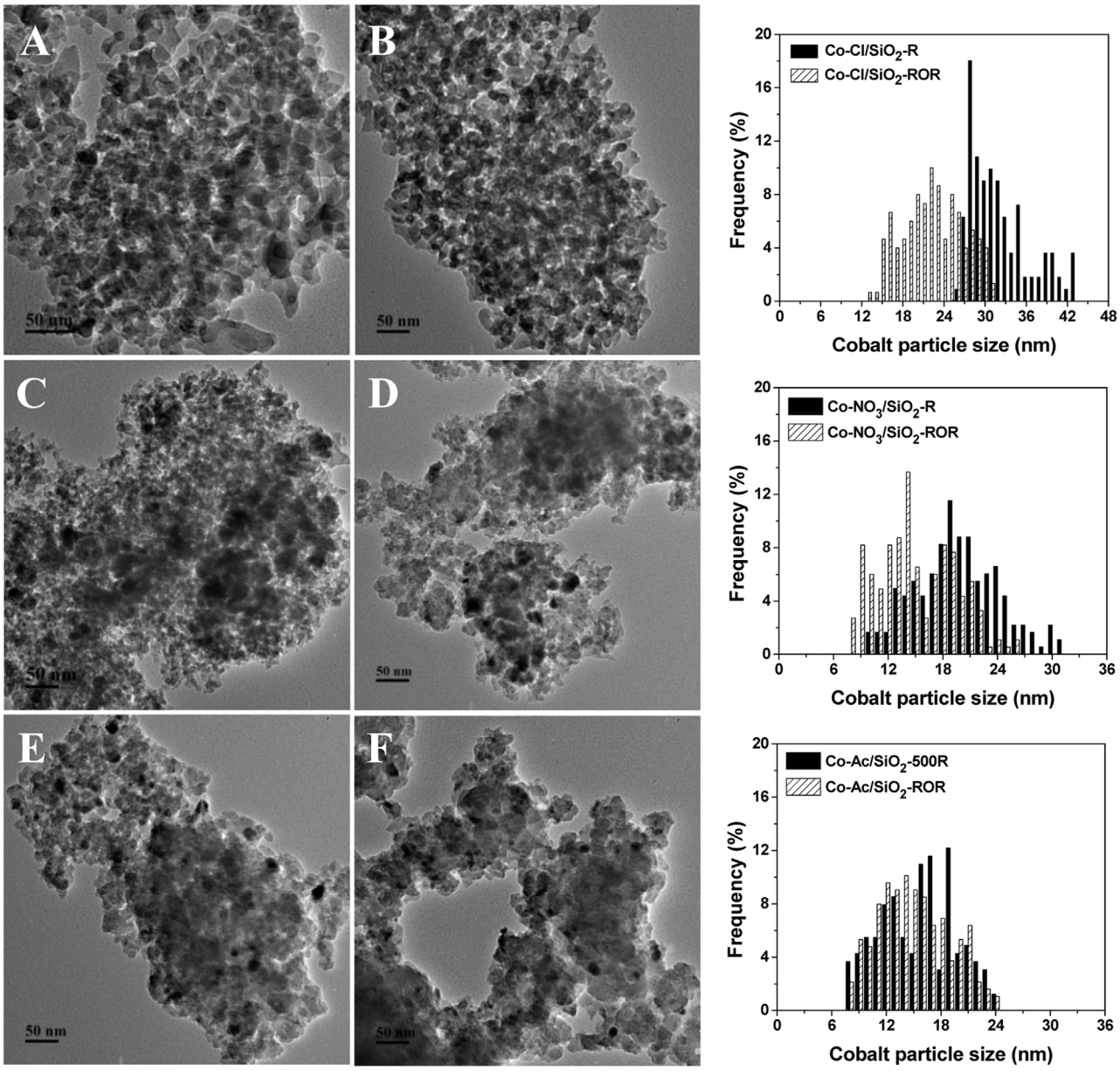

Fig. 5. TEM images and corresponding PSD of R and ROR treated samples of (A) Co-Cl/SiO_2-R, (B) Co-Cl/SiO_2-ROR, (C) Co-NO_3/SiO_2-R, (D) Co-NO_3/SiO_2-ROR, (E) Co-Ac/SiO_2-R, and (F) Co-Ac/SiO_2-ROR.

Table 3
Catalytic performance of the catalysts with different oxidation gases during the ROR treatment.[a]

Catalyst	CO conv.(%)	CO_2 sel.(%)	Hydrocarbon Selectivity (%)			
			CH_4	$C_2^=$-$C_4^=$	C_2^0-C_4^0	C_{5+}
Co/SiO_2-R	49.9	0.9	8.5	3.3	2.8	84.5
Co/SiO_2-RR	49.5	0.9	8.6	3.3	2.9	84.3
Co/SiO_2-R-N_2-R	49.2	1.0	8.1	3.5	2.9	84.5
Co/SiO_2-R-Air-R	59.3	1.1	8.7	2.4	3.3	84.4
Co/SiO_2-R-H_2O(60)-R	53.4	1.0	8.2	3.3	3.2	84.3
Co/SiO_2-R-H_2O(80)-R	44.2	0.9	9.8	4.1	3.6	81.6
Co/SiO_2-R-H_2O(100)-R	28.4	1.3	14.4	9.0	5.4	69.9

[a] Reaction conditions: 1 g of catalyst, 230 °C, 1 MPa, $H_2/CO = 2$, TOS = 10 h, GHSV = 4.5 L g_{cat}^{-1} h^{-1}.

attentions are mainly paid on the role of surface structure, support, and promoter to establish site requirements for reactant (H_2 and CO) adsorption and dissociation for subsequent formation of initial monomer and surface polymerization. Due to the complexity of surface structures and reaction pathways affected in FTS, the more precise knowledge of site requirements for FTS reaction concerning those controversial issues should be obtained to efficiently improve the application of FTS technology [31,32,37]. In order to attain this purpose of more accurately modelling FTS rates on cobalt catalysts, the typical model catalyst of 20 wt% Co/SiO_2 in the absence

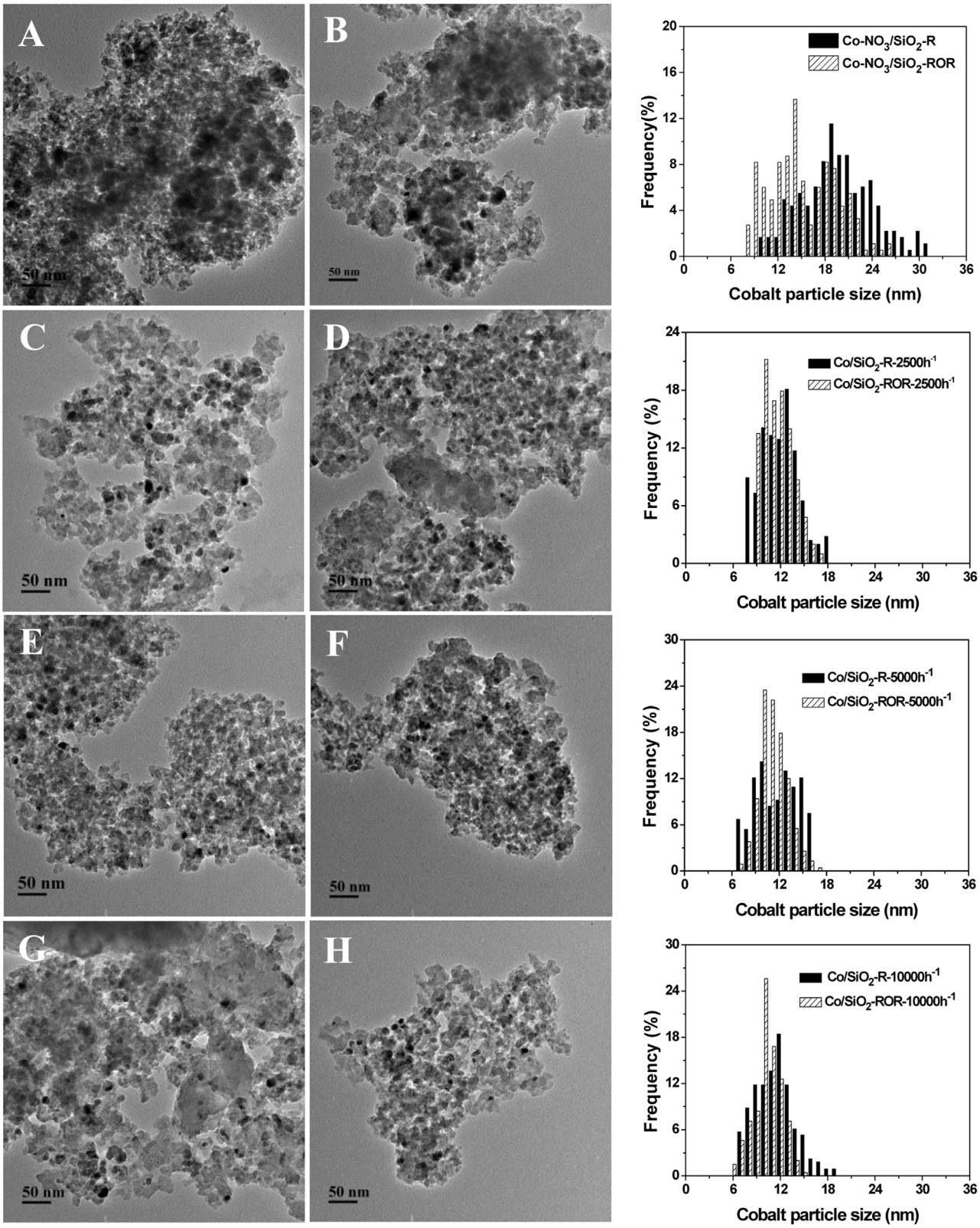

Fig. 6. TEM images and corresponding PSD of R and ROR treated samples of (A) Co/SiO_2-R, (B) Co/SiO_2-ROR, (C) Co/SiO_2-R-2500 h^{-1}, (D) Co/SiO_2-ROR-2500 h^{-1}, (E) Co/SiO_2-R-5000 h^{-1}, (F) Co/SiO_2-ROR-5000 h^{-1}, (G) Co/SiO_2-R-10,000 h^{-1}, (H) Co/SiO_2-ROR-10,000 h^{-1}.

of promoter is used to study on how the gas character, such as nitrogen, oxygen, and water vapor, affects the surface structure of support, changes the cobalt phase and nanoparticle size, and alters the reducibility of cobalt during the catalyst preparation and ROR treatment. Based on the results described above, we are trying to discuss the following several aspects.

Table 4
Effect of initial size of supported cobalt oxide on their ROR behavior in the FTS reaction.[a]

Catalyst	CO conv.(%)	CO_2 sel.(%)	Hydrocarbon Selectivity (%)			
			CH_4	$C_2^=$-$C_4^=$	C_2^0-C_4^0	C_{5+}
Co-Cl/SiO_2-R	6.5	1.4	16.4	3.6	10.4	68.2
Co-Cl/SiO_2-ROR	13.4	0.8	15.9	3.3	7.1	72.9
Co-NO_3/SiO_2-R	49.9	0.9	8.5	3.3	2.8	84.5
Co-NO_3/SiO_2-ROR	59.3	1.1	8.7	2.4	3.3	84.4
Co-NO_3/SiO_2-RORORO	60.0	1.4	8.4	2.4	3.2	84.6
Co-Ac/SiO_2-R	54.6	1.1	10.6	3.1	4.1	81.1
Co-Ac/SiO_2-ROR	56.3	1.0	10.1	2.8	3.5	83.2

[a] Reaction conditions: 1 g of catalyst, 230 °C, 1 MPa, $H_2/CO = 2$, TOS = 10 h, GHSV = 4.5 L g_{cat}^{-1} h^{-1}. The air is used as oxidant in OR treatment.

3.4.1. Working mechanisms of cobalt re-dispersion in ROR treatment over different oxidizing gases

From the results previously described, it can be known that the OR treatment obviously decreases the metallic cobalt particle size relative to that of the reduced cobalt catalysts, which is not related with the character of oxidizing gas. Namely, both water vapor and oxygen can be utilized to oxidize the metallic cobalt with subsequent reduction to form smaller cobalt particles. In order to understand the mechanism of change in the particle size, it is necessary for us to take insights into the chemical evolution process of metallic cobalt in the presence of oxidizing gas. When the oxidizing gas, such as water vapor or oxygen, is introduced into the reduced cobalt catalysts, it is evident that the oxidation of metallic cobalt must firstly occur from the crystal surface of cobalt particles as the following reaction equations:

$$Co + H_2O \rightarrow CoO + H_2 \quad (1)$$

$$Co + 1/2\,O_2 \rightarrow CoO \quad (2)$$

After the formation of a thin oxide shell with surface oxidation, further oxidation proceeds via fast outward diffusion of cobalt through the oxide shell, which is much faster than the inward diffusion of oxygen anions [38,39]. Thus, the vacancies are produced in the cobalt core and results in the voids inside the oxide shell with on-going oxidation, ultimately creating a polycrystalline oxide shell after completion of the oxidation process as reported by several authors [20,40]. Therefore, the different diffusion rates of cobalt and oxygen through oxide layer is the base of inside void formation and finally forming hollow oxide spheres. In this way, the oxidation mechanism leads to transport of cobalt away from its original location, spreading it over the support. The formed hollow sphere could break up, which leads to re-dispersion of the metallic cobalt phase. Based on the studies of ROR behavior over various cobalt catalysts with different preparation conditions, we found that the cobalt particle sizes reduced are strongly dependent of the initial particle size. The smaller initial particle size leads to the lower extent of size reduction in the cobalt particles, which can be explained that a smaller initial cobalt particle will form a lower volume inside void due to the reduced amount of inside cobalt diffused onto the outside surface of shell layer for oxidation reaction. In other words, the water and oxygen are easier to diffuse to reach the cobalt core for the smaller particles where most of metallic cobalt has been oxidized before they are moved to outside oxide layer. It becomes more difficult for smaller void formation to break up and re-disperse the cobalt phase. Seen from the data listed in Table S1, it seems that the particle size of metallic cobalt can be further reduced through OR treatment only when its initial size is larger than about 11 nm. The results displayed in Tables 1 and 2 show that the decrease of cobalt particle size in Co-NO_3/SiO_2 catalyst occurs in the oxidation process as the particle size is changed from the fresh (24.7 nm, Co_3O_4), R (20.6 nm, Co), RO (15.2 nm, Co_3O_4), to ROR treatment (15.7 nm, Co). The re-dispersion step is different from the proposed mechanism based on the Kirkendall effect that considers the re-reduction step as the cause of re-dispersion due to the break-up of formed hollow sphere [40]. Our experimental conclusion is also in accordance with the observation reported by Lovell et al. that the oxidation step determines the re-dispersion over the Ni-SiO_2 catalyst [41]. In addition, the final step of reduction seems to slightly increase the cobalt particle size, which is caused by agglomeration during the reduction process. In the case of water vapor, it is more effective to reduce the cobalt particle size in the oxidation step compared with the case of using oxygen as oxidizing gas as the Co_3O_4 particle size is 16.7 nm and 10.8 nm measured by TEM, respectively. This more efficient re-dispersion by water vapor might be ascribed to not only the void formation from cobalt diffusion during the cobalt oxidation but also the water vapor assisted strong interaction and reaction between the formed CoO with surface —OH as shown in Fig. 7. It is clear in Table 1 that the better re-dispersion of metallic cobalt can be realized by increasing evaporator temperature to result in the higher water vapor concentration in the reactor. When the chamber temperature is set at 60 °C, the cobalt particle size exhibits a value similar to the case of R-N_2 treated catalyst, which results from insufficient water vapor at such lower chamber temperature.

3.4.2. Influences of water vapor on the evolution of support structure and cobalt species

As confirmed from the data of catalytic activity, the water vapor applied to ROR treatment does always lead to lower activity in spite of better re-dispersion of cobalt phase obtained. This different influence from the ROR treatment with oxygen has spurred us into investigating what happened on SiO_2 support and consequent cobalt phase change. In order to make convincing answer for the resulting catalytic performance, we try to elucidate the change of SiO_2 and cobalt phase in the catalysts in details. Firstly, the effects of water vapor and oxygen on the surface structure are studied over SiO_2 support without cobalt loading using the same conditions as that for oxidation step in ROR treatment. As presented in Table S3, the SiO_2 treated with oxygen and various water vapor concentrations at 300 °C and atmosphere pressure shows almost no change of specific surface area and pore structure. However, the IR spectra shown in Fig. 8 indicate that oxidizing gas has significantly affected the composition of support surface groups. It is well known that the absorption peak at about 1100 cm^{-1} is assigned to the asymmetric stretching vibration of bridge Si—O. The absorption peak at about 800 cm^{-1} is assigned to symmetric bending vibrations of Si-O-Si [42]. On the other hand, the absorption peak at about 970 cm^{-1} is assigned to asymmetric stretching vibration of bridge Si—OH [43]. Relative to the fresh SiO_2 in Fig. 8a, the surface concentration of Si—OH is obviously decreased after the calcination in air (Fig. 8b). As a result, the peak belonging to the symmetric bending vibrations of Si—O—Si is remarkably strengthened due to the dehydration of Si—OH through the following reaction:

$$2Si—OH \rightarrow Si—O—Si + H_2O \quad (3)$$

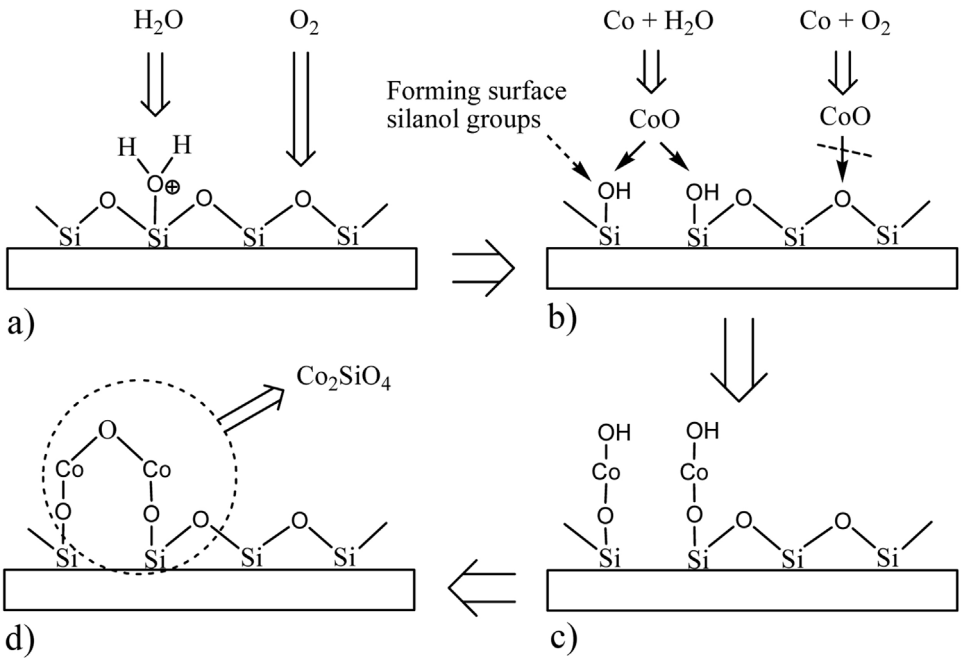

Fig. 7. Influence of oxidizing gas water vapor and O_2 on the surface structure of SiO_2 and the formation mechanism of irreducible cobalt silicate during the oxidation step in ROR treatment.

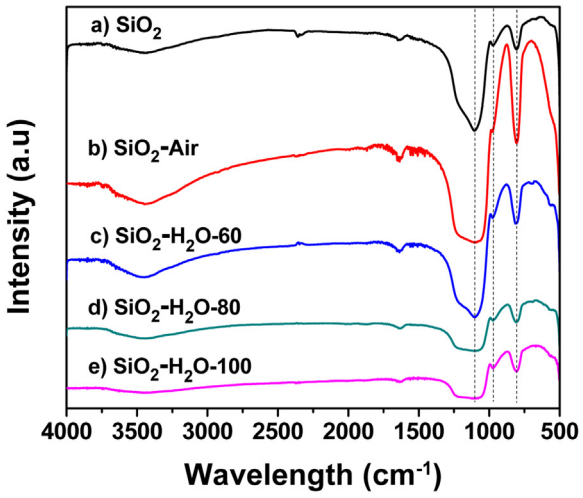

Fig. 8. IR spectra of the SiO_2 support calcined at 300 °C with air and flowing N_2 carried water vapor from vaporizer at different temperatures: a) fresh SiO_2; b) static air; c) 60 °C; d) 80 °C; e) 100 °C.

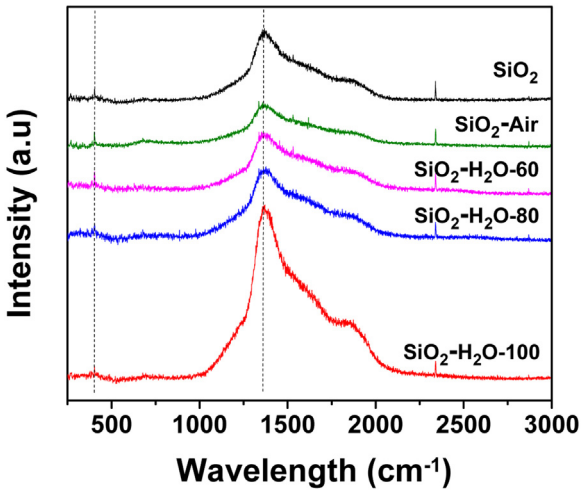

Fig. 9. Raman spectra of the SiO_2 support calcined at 300 °C in air and flowing N_2 carried water vapor from vaporizer at different temperatures: a) fresh SiO_2; b) static air; c) 60 °C; d) 80 °C; e) 100 °C.

As for the SiO_2 treated in water vapor, the ratio of peak intensity of Si-OH group to Si-O group obviously increases compared with that in air and fresh SiO_2 support, which also increases with an increase in the evaporator temperature from 60, 80 to 100 °C as shown in Fig. 8c, d, and e. Thereby, it can be deduced that the surface concentration of Si—OH group is significantly increased when the SiO_2 support is treated over the evaporator temperature higher than 80 °C. Exactly, the flow rate of water vapor is enhanced from 6.9, 32.2, to 44.8 mL/min as the evaporator temperature increases from 60, 80 to 100 °C, respectively. The influence of water vapor on the SiO_2 structure is also revealed by Raman spectra as shown in Fig. 9. As reported in literature, the Raman bound near 450 cm^{-1} is generally assigned to a symmetric oxygen vibration of bent Si—O—Si linkages. The Raman bound at 1060 cm^{-1} and 1200 cm^{-1} are assigned to asymmetric Si-O stretching vibration [44]. The Raman bound near 1300 cm^{-1} is assigned to Si=O (or Si—O^-) stretching vibration [45], which is also strengthened at higher evaporator temperature as the Si—OH group detected by IR spectra. These spectra data of IR and Raman reasonably reflects the surface structure evolution from water vapor treatment as described in Fig. 7 and the following equation:

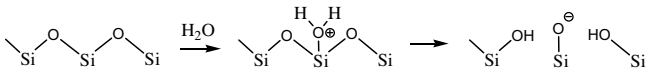

(4)

Based on the SiO_2 structure evolution over treatments in different oxidizing gases, here, we discuss the phase change of cobalt

species, namely the pathways of metallic cobalt in the first reduction step. In the case of oxygen, the metallic cobalt is firstly oxidized into CoO. Since the surface concentration of Si—OH group is remarkably reduced in the oxidation step (Fig. 8b), the CoO could not further react with Si—O—Si bond (Fig. 7b) but be oxidized into Co_3O_4. However, when the large amount of Si-OH group is available by the treatment of water vapor in oxidation step, the CoO can react with Si-OH followed by the subsequent dehydration to form the irreducible Co_2SiO_4 (Fig. 7c and d).

The fresh initial particle size of Co_3O_4 supported on the SiO_2 is changeable in a large extent by adjusting the preparation conditions. When the cobalt catalysts are prepared from the decomposition of cobalt nitrate, the enhanced presence of those moisture (i.e. water) and NO_x vapors might have caused the formation of large agglomerates of cobalt oxide crystallites [46,47]. Our results demonstrate that the removal of NO_x and H_2O decomposition products favors the formation of smaller particles, which are in line with the observations in Table S1 indicating the trend of particle size relative to the flow rate of N_2 during the calcination step. The water vapor in the preparation of catalysts favors the sintering of cobalt oxides that can also be confirmed that the smaller particles of cobalt oxide are formed by using organic impregnation solvents, such as ethanol and acetone, instead of the water [48,49]. Also, the cobalt precursors used in this study exhibit a marked impact on the particle size. The use of different salts other than nitrate results in particles of different size by changing the precursor-support interaction [50–52]. In contrast, the cobalt chloride leads to much larger particles and, however, the cobalt particles are well dispersed and smaller with cobalt acetate precursor compared with those obtained from cobalt nitrate. Tada et al. reported that residual chlorines, which originate from $HAuCl_4$, enhance the aggregation of gold nanoparticles and clusters over a reduced rutile TiO_2. The DFT calculations show Cl atoms have a stronger absorption onto a reduced TiO_2 surface thus leading to the depletion of interaction between Au and TiO_2 surface [53–55]. Therefore, the interaction between cobalt and support surface is one of the crucial factors for determining the particle size of cobalt oxide. Concerning the measurements of cobalt particles, it should be noted that XRD patterns do not exhibit the obvious diffraction peaks assigned to cobalt oxide and metallic cobalt after the reduced cobalt oxide treated with water vapor at 80 and 100 °C. This suggests that the crystallite size of cobalt oxide is below the lower limitation of XRD detectability after water vapor treatment [52]. However, the diffraction peaks assigned to cobalt oxide are still observable for the cobalt catalyst with calcination in high space velocity of flowing N_2 which leads to a similar particle size to that with water vapor treatment in the TEM images. Therefore, it is most likely that the metallic cobalt treated by water vapor does not form Co_3O_4 crystallites but may have formed an amorphous cobalt oxide. To this end, we have discussed the influence of various preparation conditions on the particle size and phase state of cobalt catalysts.

3.4.3. *Reducibility of the cobalt catalysts with preparation and ROR treatment conditions*

As reported in literature, it is well known that the reducibility of cobalt catalysts is strongly dependent of its particle size [56]. Based on the results of reducibility in this study, we try to take insights into the related aspects on how the preparation process is determining the reducibility of cobalt catalysts. As shown in Fig. 10, in the case of the cobalt catalysts prepared from different precursors, the smaller particle size for Co-AC/SiO_2 catalyst leads to a substantially lower reducibility compared to that for Co-NO_3/SiO_2 catalyst, which is in accordance with previously reported [57]. However, the Co-Cl/SiO_2 catalyst gives the lowest reducibility in spite of its largest cobalt particle size. This resulting lowest reducibility is ascribed to the residual chlorines that suppress the

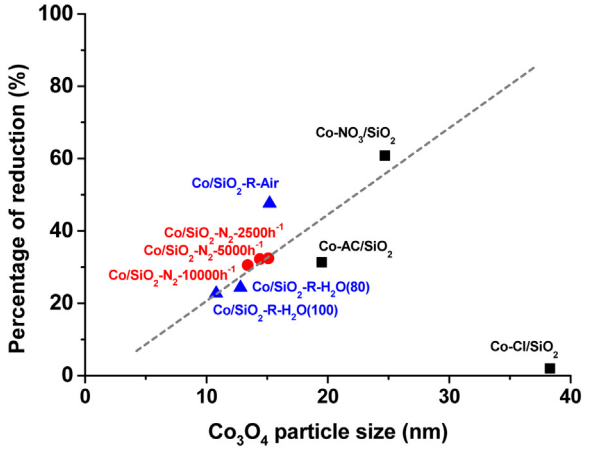

Fig. 10. Correlating the degree of reduction with Co_3O_4 particle size prepared from various precursors and treatment conditions.

reduction of cobalt oxide as confirmed in Fig. S5 that the beginning temperature of reduction peak even appears above 400 °C. For the same precursor of cobalt nitrate, the smaller particle size obtained from the calcination in flowing N_2 also results in lower reducibility compared with that in static air. Furthermore, when the reduced metallic cobalt is re-oxidized with water vapor, the cobalt phase exhibits the lowest reducibility with smallest particle size. In view of the relationship between the particle size and reducibility over the cobalt catalysts prepared from the cobalt nitrate, it is clear that the reducibility is almost linearly related to the particle size, which can fit in with the empirical equation as described below:

$$d = 96 \times (Wf)/1.179X$$

Where d = average crystallite diameters (in nanometers), X = total H_2 uptake in micromoles per gram of catalyst measured at the temperature of maximum adsorption, W = weight percentage of cobalt, and f = fraction of cobalt reduced to the metal determined from O_2 titration [56]. In particular, the value of X should be almost constant in our study for the cobalt loading, cobalt precursor and support are the same in all catalysts involved. The reducibility depending on the particle size can be explained that the contact area between the cobalt oxide and the support increases with decrease in the particle size, and thus leads to the formation of more irreducible cobalt silicate. Exactly, it is observable from Figs. 3 and S6 that the peaks at 650–750 °C assigned to irreducible cobalt silicate become stronger when the particle size decreases with the order of Co/SiO_2, Co/SiO_2-N_2, and Co/SiO_2-R-H_2O catalyst. In contrast to the Co/SiO_2-N_2 catalysts, the obviously larger particle size for Co-AC/SiO_2 does not result in a higher but similar reducibility for them as shown in Fig. 10. It can be speculated that the cobalt acetate precursor has a stronger interaction with support to form cobalt species which are more difficult to be reduced based on the results in Fig. S5. Interestingly, the Co/SiO_2-R-Air catalyst has almost the same particle size of cobalt oxide with that for Co/SiO_2-N_2-2500 h^{-1}, however, it exhibits much higher reducibility. The easier reduction for Co/SiO_2-R-Air catalyst can be deduced from the evolution process of cobalt particle size. As the cobalt particles are re-dispersed by the break-up of large hollow oxide spheres, these formed small cobalt oxide particles has a lower possibility of inter-reacting with SiO_2 surface since the calcination in air is favorable for the dehydration of Si—OH forming Si—O—Si that may not react with CoO. This explanation can also be confirmed that TPR profiles do not show the peaks assigned to the irreducible cobalt species in Fig. 3.

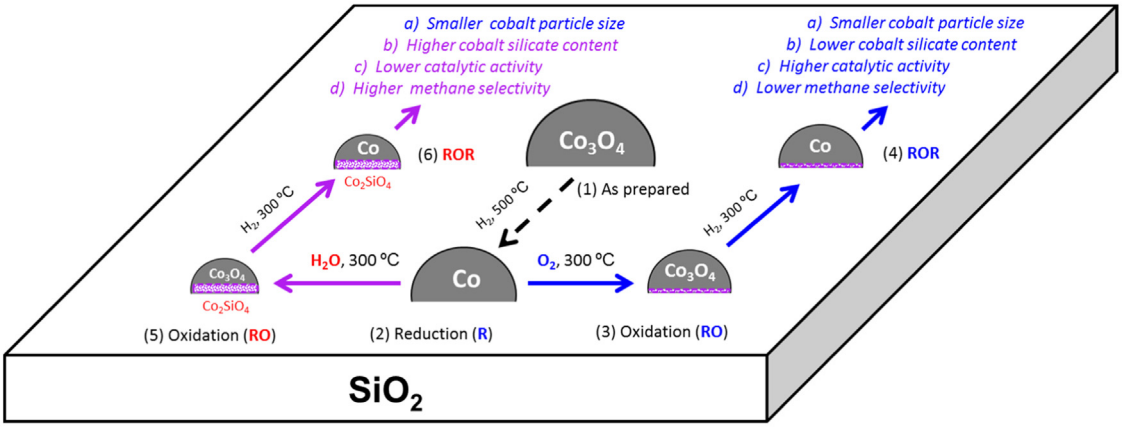

Fig. 11. Schematic representation of the effects of oxidizing gases containing water vapor and O_2 in ROR treatment on the evolution of cobalt phase and nanoparticle size.

Table 5
Influence of metallic cobalt particle size and reducibility of various prepared cobalt catalysts on the catalytic activity and selectivity of methane.

Catalyst	CO conv.(%)	CH_4 sel.(%)	d(Co)nm	Percentage of reduction(%)
Co-NO_3/SiO_2	49.9	8.5	20.6	60.8
Co-AC/SiO_2	54.6	10.6	14.7	31.3
Co-Cl/SiO_2	6.5	16.4	35.2	2.0
Co/SiO_2-R-Air	59.3	8.7	15.2	47.6
Co/SiO_2-R-H_2O(80)	44.2	9.8	9.6	24.3
Co/SiO_2-R-H_2O(100)	28.4	14.4	8.1	22.7
Co/SiO_2-N_2-2500 h^{-1}	72.3	9.1	13.1	32.4
Co/SiO_2-N_2-5000 h^{-1}	75.5	9.8	11.8	32.2
Co/SiO_2-N_2-10000 h^{-1}	79.6	9.6	10.6	30.5

Reaction conditions: 1 g of catalyst, 230 °C, 1 MPa, H_2/CO = 2, TOS = 10 h, GHSV = 4.5 L g_{cat}^{-1} h^{-1}.

3.4.4. Dependence of the catalytic performance on the cobalt particle size and reducibility

Finally, based on the understanding of evolution on the SiO_2 surface structure and cobalt phase over various processing conditions, it allows us to correlate the catalytic performances in FTS with the structure of cobalt catalysts as depicted in Fig. 11. Here, we pay more attention to discussing the influence of cobalt particle size and its reducibility on the catalytic activity and selectivity. As mentioned in the previous results [19–23], in the case of using oxygen as oxidizing gas, the ROR treatment does always lead to the enhancement of catalytic activity, and the increase in the activity mainly depends on the extent of decrease in cobalt particle size. In contrast, the water vapor utilized in the oxidation step decreases the catalytic activity in spite of much smaller cobalt particles obtained after ROR treatment, which results from the sharp decline of reducibility due to the water vapor assisted formation of irreducible cobalt silicate. Indeed, as shown in Table 3, the catalytic activity is decreased to a larger extent with the increase in the flow rate of water vapor. Table 5 displays the results of catalytic activity and selectivity of methane over different metallic cobalt particles and reducibility from various prepared cobalt catalysts. As can be observed from the data, the Co-AC/SiO_2 exhibits a higher catalytic activity compared with Co-NO_3/SiO_2 owning considerably higher reducibility, which might be due to more exposed metallic surface cobalt atoms available for FTS reaction resulting from much smaller particle size despite remarkably lower reducibility. When the cobalt catalysts have similar reducibility of about 31%–32%, the catalytic activity increases from 54.6% to 79.6% with a decrease in the cobalt particle size from 14.7 to 10.6 nm as the order of Co-AC/SiO_2, Co/SiO_2-N_2-2500 h^{-1}, Co/SiO_2-N_2-5000 h^{-1}, and Co/SiO_2-N_2-10000 h^{-1}. According to the widely accepted viewpoint, the cobalt particle size and the reducibility of cobalt are the main factors affecting methane selectivity which is also well reflected in our study [58,59]. As the Co-NO_3/SiO_2 and Co/SiO_2-R-Air catalysts have relatively larger cobalt particle sizes and higher reducibility, the lower selectivity of methane is produced compared with other cobalt catalysts except for the Co-Cl/SiO_2 catalyst in Table 5. It is reported that the trend for methane selectivity decreases when increase cobalt particle size below the critical size (ca. 8–10 nm) [10]. This conclusion can explain that the Co/SiO_2-R-H_2O (100) gives a significantly higher selectivity of methane from 9.8% to 14.4% compared to that for Co/SiO_2-R-H_2O (80) as the cobalt particle size decreases from 9.6 to 8.1 nm near the critical size. For Co-Cl/SiO_2 catalyst, although it has the largest cobalt particle size, the highest selectivity of methane is produced due to its lowest reducibility in the presence of residual chlorides [60]. Therefore, based on the above discussions related to the catalytic activity and selectivity of methane, we can draw the following points about how to improve the catalytic activity and minimize selectivity of methane: 1) to obtain the suitable cobalt particle size and efficient reduction of cobalt oxide; 2) to avoid the presence of various fouling and poisons, such as sulfur, chloride, oxidized cobalt, irreducible cobalt silicate, on the surface of metallic cobalt crystals during the catalyst preparation and FTS reaction. Additionally, it should be noted that an obvious increase in the selectivity of $C_2^=$–$C_4^=$ is observed over Co/SiO_2-R-H_2O (100)-R, which is closely related to the much smaller cobalt particle size. The results in this study are well in accordance with the changing trend that the cobalt particle size above 10 nm shows no marked effect on the selectivity of olefins and, however, the olefin selectivity rapidly increases with a decrease in the cobalt particle size below 10 nm [10].

4. Conclusions

In summary, reduction-oxidation-reduction (ROR) treatment using water vapor and oxygen as oxidizing gas has been applied in FTS to gain insights in the working catalyst. BET, XRD, TEM, H_2-TPR, FTIR, and Raman measurements are used to study the evolution of

support structure and cobalt phase and morphology at each step. Firstly, the different initial cobalt particle sizes are prepared by regulating cobalt precursors and calcination conditions (in static air and flowing N_2), which indicates that the particle size is determined by interaction between cobalt ion and SiO_2 support, and the enhanced concentration of decomposition products such as NO_x and H_2O favors the formation of larger agglomerates of cobalt oxide crystallites. Subsequently, compared to ROR treatments over these prepared cobalt catalysts, results show that ROR treated using both water vapor and oxygen as oxidizing gas exhibits a significant re-dispersion of cobalt oxide particles to form smaller size. The extent of decrease in the particle size depends on initial cobalt particle size, and only the cobalt particle above a critical size (about 11 nm) can be further reduced by ROR treatment. Furthermore, the water vapor seems to be more favorable for facilitating re-dispersion to obtain even smaller size. The ROR treatment with oxygen results in higher catalytic activity because the oxidation step in oxygen not only leads to smaller cobalt particle size but also prevents forming more irreducible cobalt silicate. However, the cobalt catalysts are obviously deactivated through the ROR treatment using water vapor as oxidizing gas in spite of smaller cobalt particle size obtained, which is ascribed to the promoted formation of cobalt silicate. The catalytic results imply that the catalytic activity is in accordance with the exposed amount of surface cobalt atoms, and the selectivity of methane depends on the cobalt particle size, the reduction degree, and the elimination of fouling and poisons on the cobalt crystal surface.

Acknowledgements

The authors wish to acknowledge the financial support from the National Natural Science Foundation of China (21576119) and the Natural Science Foundation of Jiangsu Province (BK20151125).

Appendix A. Supplementary data

Supplementary data associated with this article can be found, in the online version, at http://dx.doi.org/10.1016/j.apcatb.2017.03.036.

References

[1] G. Melaet, W.T. Ralston, C.S. Li, S. Alayoglu, K. An, N. Musselwhite, B. Kalkan, G.A. Somorjai, J. Am. Chem. Soc. 136 (2014) 2260–2263.
[2] A.T. Bell, Nature 456 (2008) 185–186.
[3] S.-H. Kang, J.W. Bae, J.-Y. Cheon, Y.-J. Lee, K.-S. Ha, K.-W. Jun, D.-H. Lee, B.-W. Kim, Appl. Catal. B: Environ. 103 (2011) 169–180.
[4] S. Janbroers, P.A. Crozier, H.W. Zandbergen, P.J. Kooyman, Appl. Catal. B: Environ. 102 (2011) 521–527.
[5] D. Lorito, C. Ruocco, V. Palma, A. Giroir-Fendler, F.C. Meunier, Appl. Catal. B: Environ. 197 (2016) 56–61.
[6] A.Y. Khodakov, W. Chu, P. Fongarland, Chem. Rev. 107 (2007) 1692–1744.
[7] E. Iglesia, Appl. Catal. A: Gen. 161 (1997) 59–78.
[8] N. Tsubaki, Y. Zhang, S.L. Sun, H. Mori, Y. Yoneyama, X.H. Li, K. Fujimoto, Catal. Commun. 2 (2001) 311–315.
[9] N. Tsubaki, S.L. Sun, K. Fujimoto, J. Catal. 199 (2001) 236–246.
[10] G.L. Bezemer, J.H. Bitter, H.P.C.E. Kuipers, H. Oosterbeek, J.E. Holewijn, X.D. Xu, F. Kapteijn, A.J. van Dillen, K.P. de Jong, J. Am. Chem. Soc. 128 (2006) 3956–3964.
[11] A.M. Saib, A. Borgna, J.V. de Loosdrecht, P.J. van Berge, J.W. Niemantsverdriet, Appl. Catal. A: Gen. 312 (2006) 12–19.
[12] A.M. Saib, D.J. Moodley, I.M. Ciobica, M.M. Hauman, B.H. Sigwebela, C.J. Weststrate, J.W. Niemantsverdriet, J. van de Loosdrecht, Catal. Today 154 (2010) 271–282.
[13] D. Schanke, A.M. Hilmen, E. Bergene, K. Kinnari, E. Rytter, E. Adnanes, A. Holmen, Energy Fuel 10 (1996) 867–872.
[14] P.J. van Berge, J. van de Loosdrecht, S. Barradas, A.M. van der Kraan, Catal. Today 58 (2000) 321–334.
[15] N.E. Tsakoumis, M. Ronning, O. Borg, E. Rytter, A. Holmen, Catal. Today 154 (2010) 162–182.
[16] G.L. Bezemer, T.J. Remans, A.P. van Bavel, A.I. Dugulan, J. Am. Chem. Soc. 132 (2010) 8540–8541.
[17] D.J. Moodley, J. van de Loosdrecht, A.M. Saib, M.J. Overett, A.K. Datye, J.W. Niemantsverdriet, Appl. Catal. A: Gen. 354 (2009) 102–110.
[18] S.L. Soled, E. Iglesia, R.A. Fiato, J.E. Baumgartner, H. Vroman, S. Miseo, Top. Catal. 26 (2003) 101–109.
[19] P.A. Chernavskii, G.V. Pankina, M.I. Ivantsov, A.Y. Khodakov, Russ. J. Phys. Chem. A 87 (2013) 1349–1352.
[20] S. Sadasivan, R.M. Bellabarba, R.P. Tooze, Nanoscale 5 (2013) 11139–11146.
[21] L.G. Tang, D. Yamaguchi, B. Leita, V. Sage, N. Burke, K. Chiang, Catal. Commun. 59 (2015) 166–169.
[22] M.M. Hauman, A. Saib, D.J. Moodley, E. du Plessis, M. Claeys, E. van Steen, ChemCatChem 4 (2012) 1411–1419.
[23] C.J. Weststrate, A.M. Saib, J.W. Niemantsverdriet, Catal. Today 215 (2013) 2–7.
[24] G. Jacobs, A. Sarkar, Y.Y. Ji, M.S. Luo, A. Dozier, B.H. Davis, Ind. Eng. Chem. Res. 47 (2008) 672–680.
[25] S. Lögdberg, D. Tristantini, Ø. Borg, L. Ilver, B. Gevert, S. Järås, E.A. Blekkan, A. Holmen, Appl. Catal. B: Environ. 89 (2009) 167–182.
[26] S.K. Beaumont, Phys. Chem. Chem. Phys. 16 (2014) 5034–5043.
[27] S. Storsaeter, O. Borg, E.A. Blekkan, A. Holmen, J. Catal. 231 (2005) 405–419.
[28] X.H. Liu, M. Tokunaga, ChemCatChem 2 (2010) 1569–1572.
[29] X.H. Liu, W.S. Linghu, X.H. Li, K. Asami, K. Fujimoto, Appl. Catal. A: Gen. 303 (2006) 251–257.
[30] G. Jacobs, Y.Y. Ji, B.H. Davis, D. Cronauer, A.J. Kropf, C.L. Marshall, Appl. Catal. A: Gen. 333 (2007) 177–191.
[31] E. vanSteen, G.S. Sewell, R.A. Makhothe, C. Micklethwaite, H. Manstein, M. deLange, C.T.O. Connor, J. Catal. 162 (1996) 220–229.
[32] J.H. den Otter, S.R. Nijveld, K.P. de Jong, ACS Catal. 6 (2016) 1616–1623.
[33] X.H. Liu, X.H. Li, Y. Suehiro, K. Fujimoto, Appl. Catal. A: Gen. 333 (2007) 211–218.
[34] C.I. Ahn, H.M. Koo, J.M. Jo, H.S. Roh, J.B. Lee, Y.J. Lee, E.J. Jang, J.W. Bae, Appl. Catal. B: Environ. 180 (2016) 139–149.
[35] T.O. Eschemann, W.S. Lamme, R.L. Manchester, T.E. Parmentier, A. Cognigni, M. Ronning, K.P. de Jong, J. Catal. 328 (2015) 130–138.
[36] G. Prieto, A. Martinez, P. Concepcion, R. Moreno-Tost, J. Catal. 266 (2009) 129–144.
[37] D. Varisli, N.G. Kaykac, Appl. Catal. B: Environ. 127 (2012) 389–398.
[38] H.J. Fan, U. Gcsele, M. Zacharias, Small 3 (2007) 1660–1671.
[39] N. Caberra, N.F. Mott, Rep. Prog. Phys. 12 (1949) 163–184.
[40] A.M. Saib, J.L. Gauché, C.J. Weststrate, P. Gibson, J.H. Boshoff, D.J. Moodley, Ind. Eng. Chem. Res. 53 (2014) 1816–1824.
[41] E.C. Lovell, A. Fuller, J. Scott, R. Amal, Appl. Catal. B: Environ. 199 (2016) 155–165.
[42] M. Leśniak, J. Partyka, K. Pasiut, M. Sitarz, J. Mol. Struct. 1126 (2016) 240–250.
[43] H.S. Liu, L.S. Wang, C.H. Jiang, D.D. Liu, Y.G. Jiang, B.J. Wu, Y.Q. Ji, Acta Opt. Sin. 10 (2013) 308–313.
[44] M. Okuno, B. Reynard, Y. Shimada, Y. Syono, C. Willaime, Phys. Chem. Miner. 26 (1999) 304–311.
[45] J. Cao, Z.H. Zhang, C. Xu, Chin. J. At. Mol. Phys. 28 (2011) 31–35.
[46] J.R.A. Sietsma, J.D. Meeldijk, J.P. den Breejen, M. Versluijs-Helder, A.J. van Dillen, P.E. de Jongh, K.P. de Jong, Angew. Chem. Int. Ed. 46 (2007) 4547–4549.
[47] J. van de Loosdrecht, S. Barradas, E.A. Caricato, N.G. Ngwenya, P.S. Nkwanyana, M.A.S. Rawat, B.H. Sigwebela, P.J. van Berge, J.L. Visagie, Top. Catal. 26 (2003) 121–127.
[48] W.G. Zhou, J.Y. Liu, X. Wu, J.F. Chen, Y. Zhang, Catal. Commun. 60 (2015) 76–81.
[49] X.H. Liu, B.S. Hu, K. Fujimoto, M. Haruta, M. Tokunaga, Appl. Catal. B: Environ. 92 (2009) 411–421.
[50] M. Kraum, M. Baerns, Appl. Catal. A: Gen. 186 (1999) 189–200.
[51] J. van de Loosdrecht, M. van der Haar, A.M. van der Kraan, A.J. van Dillen, J.W. Geus, Appl. Catal. A: Gen. 150 (1997) 365–376.
[52] J. Panpranot, S. Kaewkun, P. Praserthdam, J.G. Goodwin, Catal. Lett. 91 (2003) 95–102.
[53] K. Tada, K. Sakata, Y. Kitagawa, T. Kawakami, S. Yamanaka, M. Okumura, Chem. Phys. Lett. 579 (2013) 94–99.
[54] K. Tada, K. Sakata, S. Yamada, K. Okazaki, Y. Kitagawa, T. Kawakami, S. Yamanaka, M. Okumura, Mol. Phys. 112 (2013) 365–378.
[55] H. Sakurai, K. Koga, Y. Iizuka, M. Kiuchi, Appl. Catal. A: Gen. 462–463 (2013) 236–246.
[56] R.C. Reuel, C.H. Bartholomew, J. Catal. 85 (1984) 63–77.
[57] L.S. Yu, X.H. Liu, Y.Y. Fang, C.L. Wang, Y.H. Sun, Fuel 112 (2013) 483–488.
[58] D. Wang, C.B. Chen, J.G. Wang, L.T. Jia, B. Hou, D.B. Li, Appl. Catal. A: Gen. 527 (2016) 60–71.
[59] G. Prieto, M.I.S. De Mello, P. Concepción, R. Murciano, S.B.C. Pergher, A. Martínez, ACS Catal. 5 (2015) 3323–3335.
[60] Q.H. Zhang, J.C. Kang, Y. Wang, ChemCatChem 2 (2010) 1030–1058.